

PAPER • OPEN ACCESS

Sperm motility in modulated microchannels

To cite this article: Sebastian Rode *et al* 2019 *New J. Phys.* **21** 013016

View the [article online](#) for updates and enhancements.



IOP | ebooks™

Bringing you innovative digital publishing with leading voices to create your essential collection of books in STEM research.

Start exploring the collection - download the first chapter of every title for free.



PAPER

Sperm motility in modulated microchannels

OPEN ACCESS

RECEIVED
3 August 2018REVISED
17 November 2018ACCEPTED FOR PUBLICATION
30 November 2018PUBLISHED
18 January 2019

Original content from this work may be used under the terms of the [Creative Commons Attribution 3.0 licence](#).

Any further distribution of this work must maintain attribution to the author(s) and the title of the work, journal citation and DOI.

Sebastian Rode, Jens Elgeti¹ and Gerhard Gompper

Theoretical Soft Matter and Biophysics, Institute of Complex Systems and Institute for Advanced Simulation, Forschungszentrum Jülich, D-52425, Jülich, Germany

¹ Author to whom any correspondence should be addressed.E-mail: s.rode@fz-juelich.de, j.elgeti@fz-juelich.de and g.gompper@fz-juelich.de**Keywords:** sperm, confinement, microchannels, hydrodynamics, steric interactions, three-dimensional flagellar beatSupplementary material for this article is available [online](#)**Abstract**

Sperm cells swim through the fluid by a periodic wave-like beating of their flagellum. At low Reynolds numbers and in confinement, the directed motion of sperm and other microswimmers is strongly influenced by steric and hydrodynamic wall interactions. We model sperm motility in mesoscale hydrodynamics simulations by imposing a planar traveling bending wave along the flagellum. Sperm are simulated swimming in curved, straight, shallow and zigzag-shaped microchannels. Changes in the sidewall modulations and the imposed beat pattern allow the identification of a strong dependence of the surface attraction on the beat-shape envelope of the sperm cell. For swimming in zigzag microchannels, the deflection-angle distribution at sharp corners is calculated and found to be in good agreement with recent microfluidic experiments. The simulations reveal a strong dependence of the deflection angle on the orientation of the beat plane with respect to the channel sidewall, and thus deepen the understanding of sperm navigation under strong confinement. Detachment of sperm, while swimming along curved walls, is dominated by the change of beat-plane orientation. Therefore, either the emergence of a nonplanar component of the flagellar beat with increasing wavelength or the strong confinement in shallow channels drastically increases wall attraction. Our simulation results reveal a consistent picture of passive sperm guidance that is dominated by the steric interactions of the beat pattern with the nearby surfaces.

1. Introduction

Sperm propel themselves through a fluid by a periodic wave-like beat of their long and thin flagellum [1]. The traveling wave breaks time-reversal symmetry, leading to unidirectional swimming motion. Sperm consist of a passive head of large radius ($\approx 3 \mu\text{m}$), followed by a long (35–250 μm), tube-like flagellum with a small radius (250 nm–1 μm). While the underlying cellular structure is highly conserved across animal species, the length, beat shape and beat frequency vary significantly [2]. The purpose of sperm is to transport male DNA to the female egg cell for fertilization. In order to reach the egg cell, sperm need to find it and modify its direction of motion accordingly. Several biophysical mechanisms play a significant role in the navigation of the sperm cell.

In active guidance—like chemotaxis—the sperm cell registers an external signal (the chemical concentration) and adapts the beat pattern in order to steer uphill in the gradient [3, 4]. Passive guidance, on the other hand, relies solely on given sperm shape and beat pattern, and the physical effects of the surroundings. Rheotaxis [5, 6], where the sperm orients against a flow gradient, is such a passive guidance effect: similar to a flag in the wind, the flagellum is rotated against the flow [7]. Because mammalian sperm swim in closed confinement of the winded Fallopian tube, interactions with boundaries provide another important mechanism for active or passive guidance. Early works of Rothschild *et al* [8] already suggested hydrodynamic interactions as the cause for the enhanced density of bull sperm near glass plates. As pusher-type swimmers, sperm show a hydrodynamical attraction to planar walls [9]. Strong confinement of sperm in microratchets [10], rectangular straight [11] and branched channels [12] has been shown to be a useful tool in directing, sorting and selecting

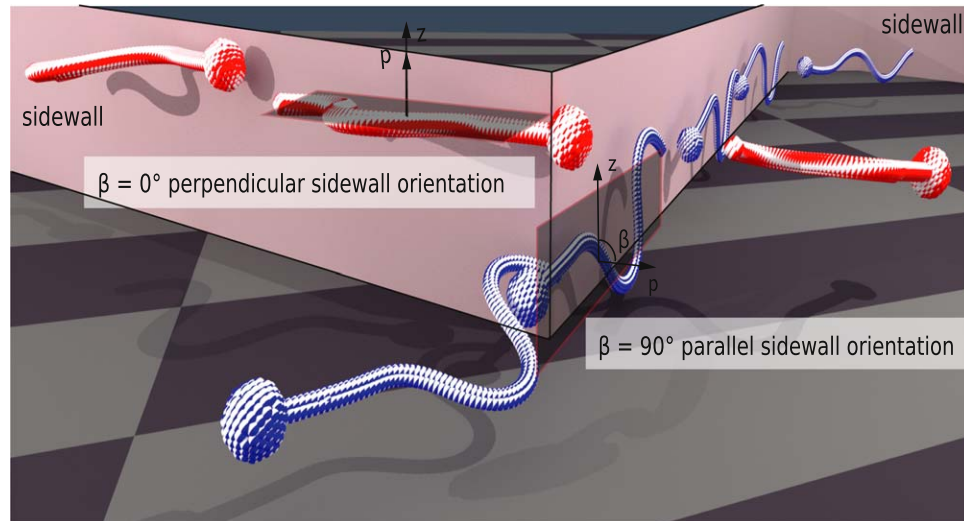


Figure 1. Parallel/perpendicular beat plane orientation—Overlay of a sperm cell swimming along the sidewall of a zigzag channel with parallel (blue) and perpendicular (red) beat-plane orientation to the sidewall. Note that the beat-plane orientation angle β is defined by the z -axis and the normal vector \mathbf{p} of the beat-plane. See also supplementary movie 1.

sperm based on their DNA integrity. Several recent experiments studied sperm in detail in modulated microchannels [10, 13]. Sperm align and swim along the sidewalls. Notably, sperm swimming in zigzag-like channels scatter off rectangular corners in fan-like trajectories [14, 15].

In this work, we focus on passive guidance of sperm by solid boundaries. We implement a minimalistic sperm model, where the flagellum beats with a predefined beat pattern. When sperm approach walls, hydrodynamic and steric interactions influence the trajectory (figure 1 and supplementary movie 1 available online at stacks.iop.org/NJP/21/013016/mmedia). Our simulations reproduce the fan-like deflection-angle distribution in zigzag channels observed experimentally. We establish a simplified steric model that explains the ensemble dynamics of the deflection process, and use it to design channels with curved regions to tune wall attraction based upon the beat pattern.

2. Models and methods

2.1. Sperm model

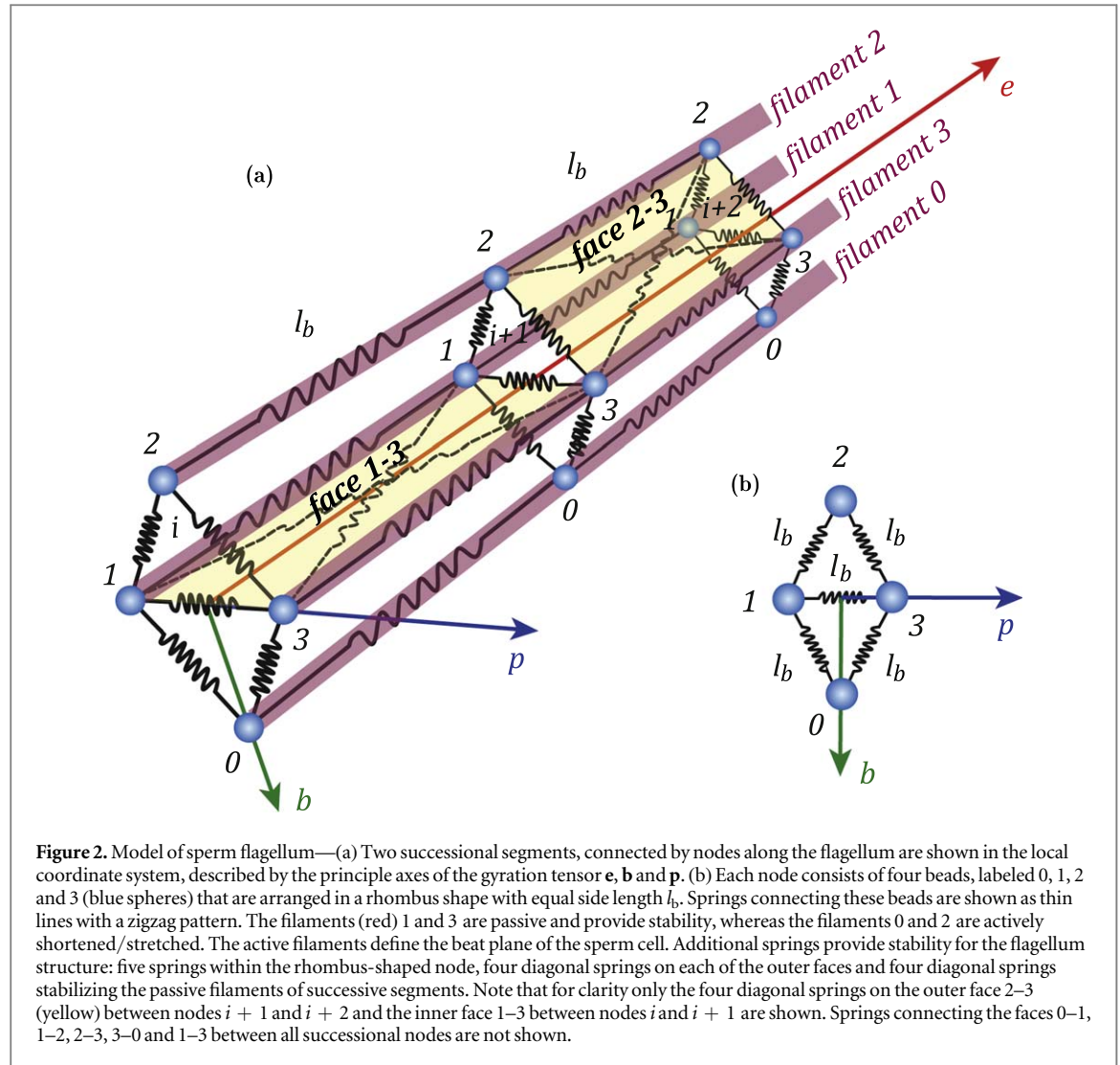
Although the specific structure of sperm cells differs from species to species, it shows many common features. The genetic material is located in a relatively large head, which is pushed through the fluid by the much longer but thinner flagellum. We base our sperm model on an elasto-mechanical description, which demonstrated realistic trajectories in bulk and close to planar walls previously [16].

The flagellum is constructed from four semi-flexible filaments, two of them passive, two active (figure 2). Each filament consists of $N_f = 100$ points which are connected by stiff springs of bond length $l_b = 0.5 a$, where a is a length scale of the simulation (see section 2.3). This results in a flagellum of arc length $L = 50 a$, that is composed of 100 nodes of rhombus shape with side length l_b . The two passive and the two active filaments oppose each other rendering the structure symmetric with respect to the center of the cross section. Additional diagonal springs stabilize the structure (see figure 2 for details).

The head of the sperm cell is approximated by a sphere of radius $r_h = 2 a$. It is modeled by $N_b = 163$ beads with one bead in the center and 162 beads uniformly covering the surface of the sphere. All surface beads are connected to their next neighbors forming a triangulated dense mesh. They are also connected to the center bead. The first four nodes of the flagellum are inside the head. Springs connect each filament of the flagellum with two beads of the sphere. The first bead of each filament is connected to the center bead, while the fourth bead of each filament is connected to the closest bead on the surface of the sphere. Due to the two-point connection the flagellum can rotate independently from the head along the central axis \mathbf{e} . A full list of parameters is presented in the appendix C.

2.2. Beat pattern

The beat pattern is imposed along the flagellum by changing the bond lengths of the two active filaments l_i^j ($j = 0, 2$), whereas the bond lengths of filament 1 and 3 are kept constant at the average bond-length value l_b .



In order to create active beating of the flagellum, the equilibrium length of the active springs

$$l_i^j = l_b \pm A \sin\left(\frac{2\pi}{\lambda} l_b i - \omega t\right) \quad (1)$$

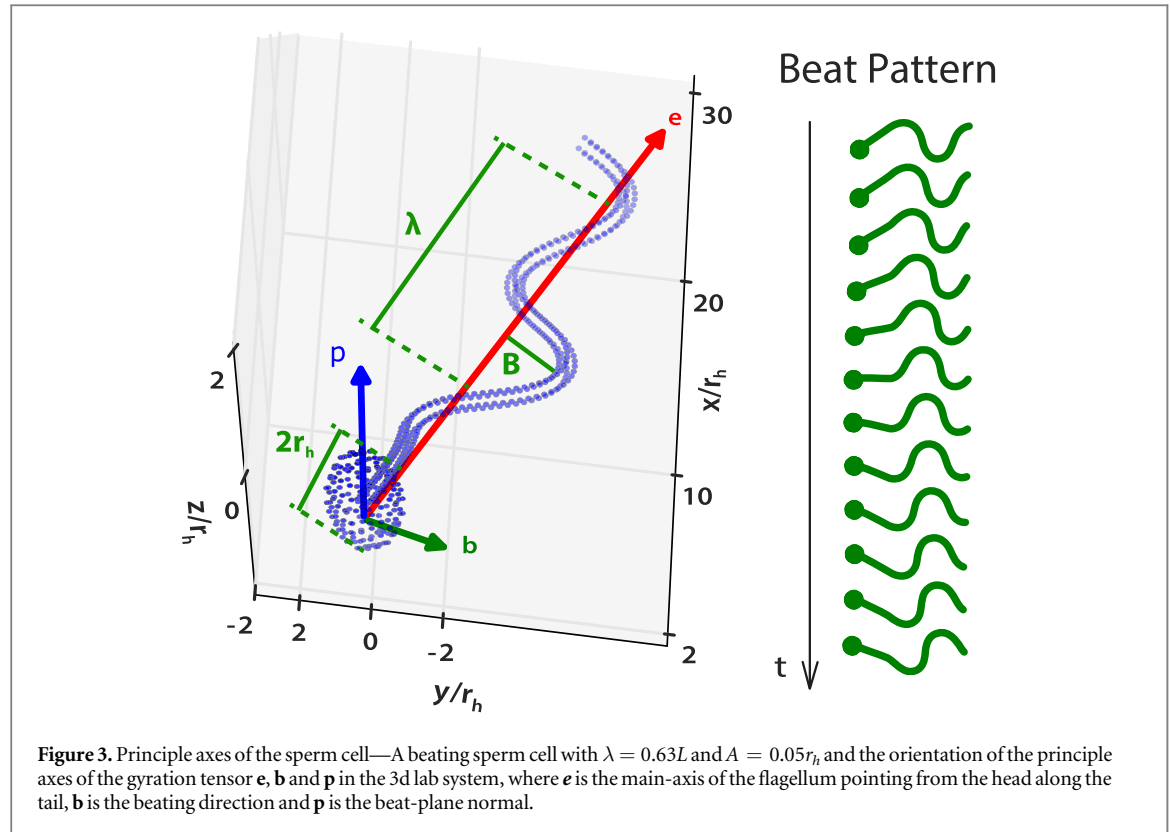
varies periodically, where i is the segment index, which increases along the arc length, A is the amplitude, λ is the wavelength and $\omega = 2\pi/\tau_b$ is the frequency of the beat. This modulation induces bending torques along the flagellum [17] that produce the beat shape. No activity is imposed along the first 20 nodes ($i \leq 20$), in order to model the stiff midpiece of sperm. Diagonal springs connecting active and passive filaments are diagonals of isosceles trapezoids. Accordingly their equilibrium length follows as $\sqrt{l_b^2 + l_b(l_i^j)^2}$.

For $\omega \neq 0$, the difference in imposed equilibrium curvature and actual curvature of the flagellum leads to effective torques which bend the flagellum. Due to the anisotropic friction in the hydrodynamic solvent, a propagating sinusoidal bending wave leads to forward swimming, where the average swimming velocity scales as $v \propto A^2 \omega \lambda^3$ [18].

We characterize the instantaneous configuration of the flagellum by the position of its centroid and the three principle axes of the gyration tensor of the flagellum (figure 3). The active filaments ($j = 0, 2$) define the beat plane, which is characterized by the beat-plane normal \mathbf{p} .

2.3. Hydrodynamic simulation

Hydrodynamic interactions with the walls and between the beads of the sperm model are introduced by using multi particle collisions dynamics (MPC) [19, 20], a mesoscale hydrodynamic simulation technique. This method has been employed for hydrodynamic descriptions of various biological microswimmers in recent years [9]. The main advantage of this method for this study is an easy implementation of complex boundaries. MPC is a particle-based simulation method allowing for highly parallelized, efficient simulations. The fluid consists of an ensemble of point particles of mass m . Successively, in each time-step, a collision and streaming step is



performed. In the streaming step, each fluid particle is moving ballistically according to its velocity. Particles interact only in the collision step on a box level. Particles are sorted into the boxes of a cubic lattice with lattice constant a . All particles in a box exchange momentum such that the center of mass velocity of the entire box is conserved. For each box a random axis is chosen around which the relative velocities of the particles are rotated by a fixed collision angle of 130° . This introduces noise and long-range hydrodynamic correlations between particles. Coupling between fluid and sperm motions is achieved by integrating the sperm beads ($m_{\text{MD}} = 5m$) into the MPC collision step. The dynamics of the beads of the sperm cell are integrated using a classical velocity-Verlet algorithm.

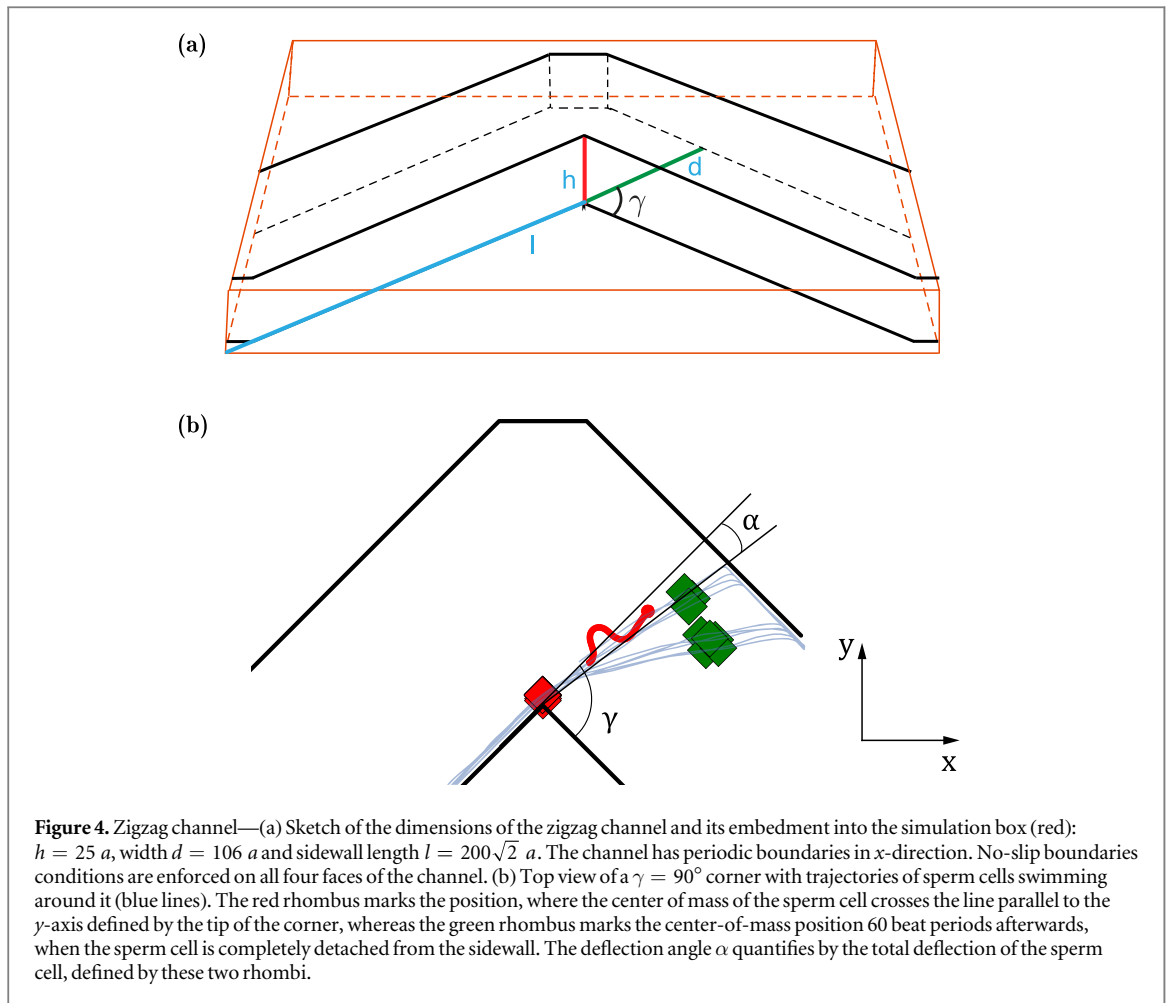
Here, we use a mean free path length $\lambda_p = 0.05 a$, a fluid density of $\rho = 10 a^{-3}$ particles per box. This ensures fluid-like behavior. The temperature of the fluid is regulated by a global thermostat to $k_b T$. Length and energies are measured in units of a and $k_b T$, receptively, which corresponds to setting $a = 1$, $m = 1$ and $k_b T = 1$.

Along the x -direction of the cubic simulation box, we impose periodic boundaries. No slip at the sidewalls is implemented via bounce-back boundary conditions and virtual wall particles [21]. Whereas the no-slip wall along the z -direction is planar, the sidewall orientation of the channel varies periodically. Therefore, the bounce-back at the sidewall is implemented in a simplified form by inverting the fluid particle velocity just before wall crossing.

2.4. Channel geometry

We first study sperm swimming along the sidewall of a zigzag channel with corner angle γ (figure 4). The cubic simulation box has the dimensions $L_x = 400 a$, $L_y = 400 a$ and $L_z = 25 a$ with periodic boundaries along the x -direction. The specific channel pattern is embedded in the simulation box and limits the motion in y -direction by two sidewalls, which are separated by a normal distance of $35.4 r_h$. The zigzag channel has a height $h = 25 a$, width $d = 106 a$ and sidewall length $l = 200\sqrt{2} a$ (see also appendix C). The zigzag channel is reconstructed with the same aspect ratio, as used in the experiments of Kantsler *et al* [15].

In the second setup, we smooth the corner by replacing the sharp corner with a quarter-circles of constant radius of curvature R . Straight parts connect the alternating quarter circles. Thereby, the curved channel remains similar to the alternating pattern of the zigzag channel.



3. Results

3.1. Zigzag channels

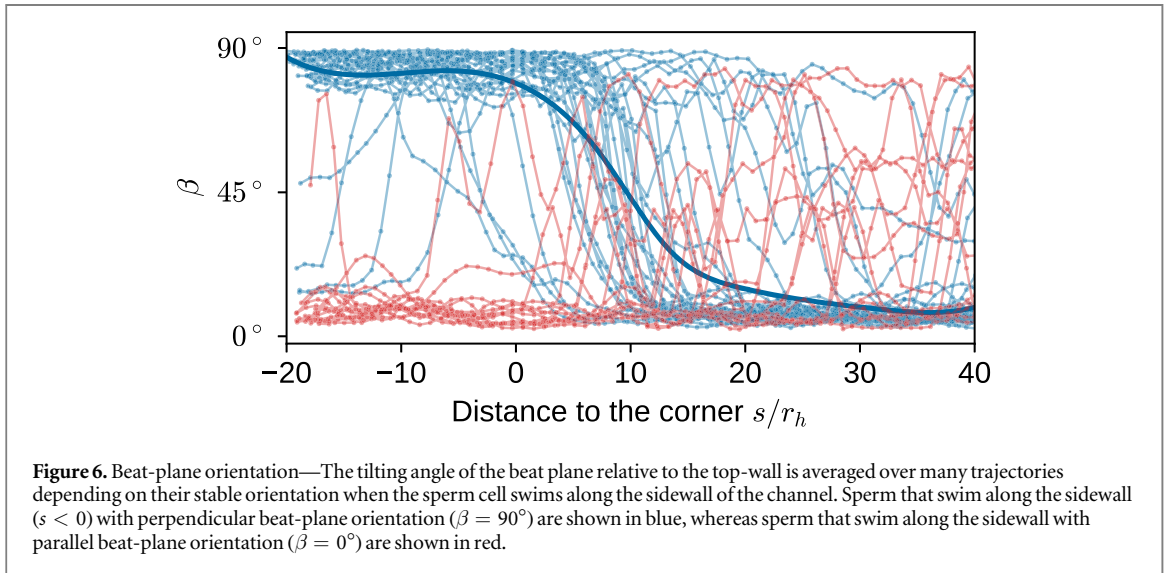
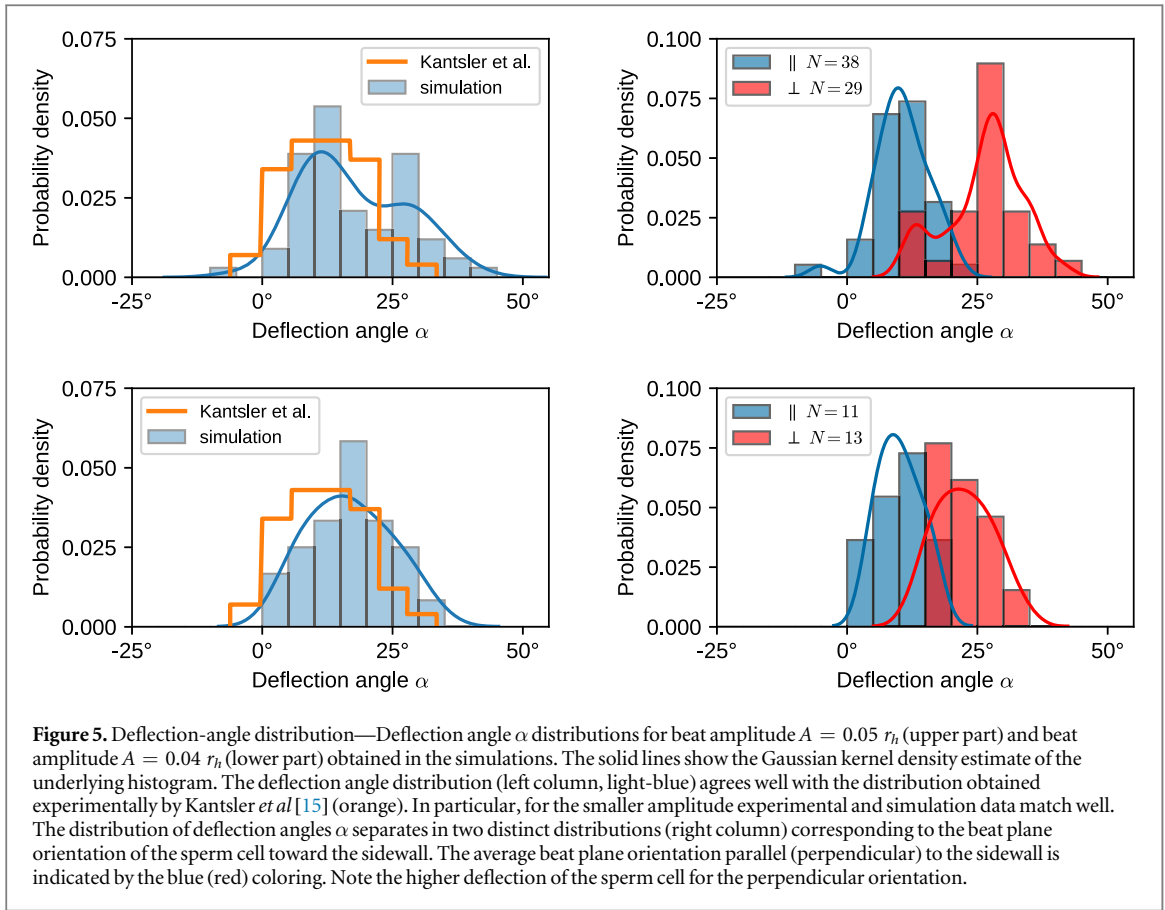
We simulate sperm swimming in zigzag channels with $\gamma = 90^\circ$ corners (supplementary movie 1). The sperm beat with a wavelength $\lambda = 0.63 L$ and a beat frequency $\omega = 0.05 \sqrt{k_B T / (a^2 m)}$ at two different beat amplitudes $A = 0.05 r_h$ and $A = 0.04 r_h$. The choice of wavelength, and in particular $\lambda < L$, is based upon previous work on tethered sperm [17], where this wavelength reproduces experimentally observed beat patterns very well. The chosen beat frequency ensures both low-Reynolds-number dynamics with negligible inertia effects and reasonable simulation run times.

Typical trajectories and their deflection angles are shown in figure 4. Sperm follow the sidewall—until they detach at the tip of the corner, cross the channel and reorient along the opposing sidewall. The deflections show a large spread for different realizations. Note that the reorientation happens while the flagellum stays in contact with the sidewall. After it loses contact, the trajectory becomes almost straight. This already hints an important result of this work, which we will strengthen further through this paper: the instantaneous beat shape of the sperm cell crucially determines the outcome of the deflection.

For a more quantitative analysis, the deflection angle α is defined as the turning of the sperm cell between the position when the center of the head is at the tip of the corner and its position 60 beats afterwards, when the entire sperm cell is detached from the sidewall. When sperm do not change swimming direction, they continue to swim along the extension of the sidewall. This corresponds to $\alpha = 0$. Turning around the corner toward the originating sidewall is defined as a positive α , whereas turning away from the sidewall extension is defined as a negative α (figure 4).

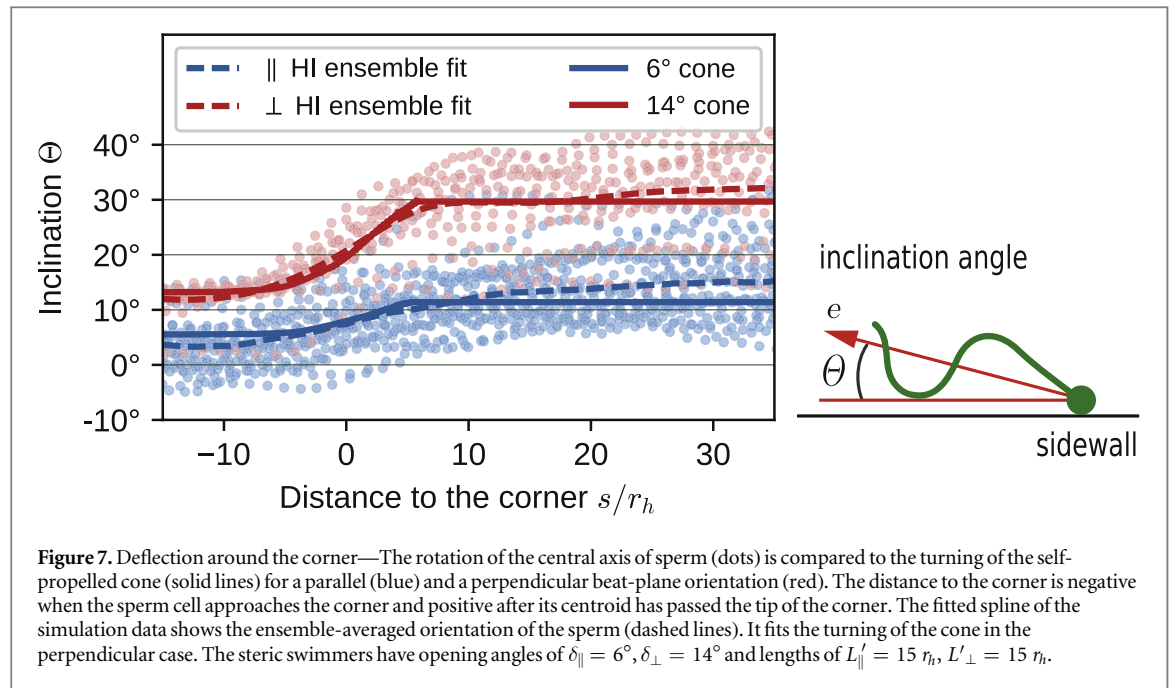
The simulated trajectories for $A = 0.05 r_h$ imply that the mean deflection angle is positive, $\langle \alpha \rangle \approx 15^\circ$, with a very broad distribution from slightly negative α up to $\alpha = 45^\circ$ (figure 5).

Nevertheless, even for the large deflections, the sperm cell always crosses the channel and reaches the opposing side, i.e. it never sneaks around the corner. For the larger beat amplitude, $A = 0.05 r_h$ two distinct peaks can be identified, whereas the sperm with smaller beat amplitude $A = 0.04 r_h$ show a distribution with a single peak that fits the experimental data very well. As shown previously in simulations [16], sperm orient their



beat plane parallel to a nearby no-slip wall. Therefore, sperm either align parallel to the sidewalls, or to the top/bottom walls of the channel. Indeed, we observe an almost bimodal distribution of the beat plane orientation (figure 6). Hence alignment is either defined as parallel, with $|\langle p_z \rangle| < 0.7$, or perpendicular, with $|\langle p_z \rangle| \geq 0.7$ (see also figure 1). \mathbf{p} is the beat-plane normal, as defined in section 2.2. We can thus correlate the deflection angle with the beat plane orientation.

When the sperm cell detaches from the sidewall with a previously parallel orientation, it very quickly reorients its beat plane parallel to the top (or bottom) walls (figure 6). This remarkable stability of the beat-plane orientation justifies the classification of the beat plane by its orientation with respect to either the sidewall (parallel) or the top/bottom wall (perpendicular). This classification separates the deflection-angle distribution in two reasonably well separated peaks (figure 5). The parallel beat-plane orientation results in small deflections $\langle \alpha_{\parallel} \rangle \approx 10 \pm 5^\circ$ independently of the beat amplitude, whereas the perpendicular beat-plane



orientation results in larger deflections. The perpendicular deflection-angle distribution shifts from $\langle \alpha_{\perp} \rangle \approx 26 \pm 7^\circ$ to $\langle \alpha_{\perp} \rangle \approx 22 \pm 5^\circ$ with decreasing beat amplitude.

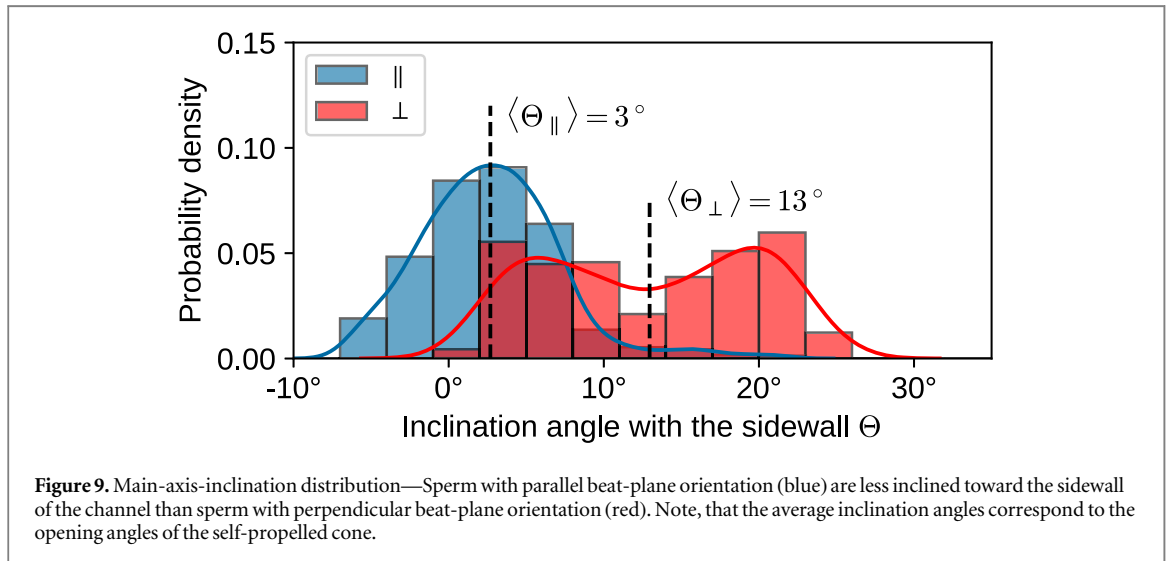
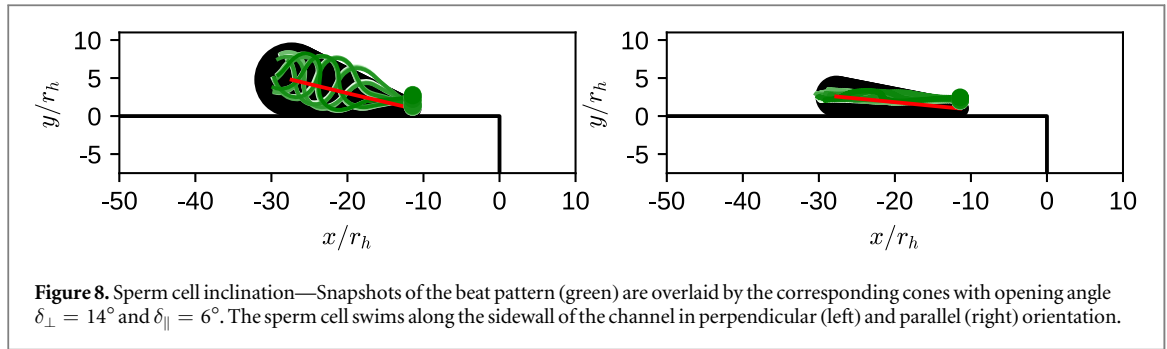
The fans of sperm cell trajectories scattering off the corner of the channel look very similar to the experimental observations of human sperm [14]. The distribution of deflection angles α of the lower sperm beat amplitude (figure 5) matches with the experimental deflection data of bull sperm [15] very well. The shift of the deflection angle distribution with perpendicular beat-plane orientation towards smaller deflections leads to a strong overlap with the distribution of the parallel case and results in a unimodal distribution, where the two contributions cannot be distinguished without additional information of the corresponding sperm cell orientation. Interestingly, the beat shape influences the deflection only in the case of a perpendicular beat-plane orientation. This suggests, a central role of steric interactions between the beating flagellum and the wall, which we will investigate further in the following section.

3.2. Self-propelled cone model

If the sperm motion were mainly determined by the average beat envelope of the flagellum, a simpler model might capture the physics of deflection of a sperm-cell ensemble. Thus, we compare the full hydrodynamic simulation of sperm to an overdamped dynamics simulation of a self-propelled cone-like particle (for details see appendix B). The cone shape is based on the form of the average beat shape envelope of the sperm. Its shape is described by two parameters: the opening angle δ and the length L' of the cone. Cones with different opening angles are constructed for both beat-plane orientations.

For a detailed comparison, we refine our quantification of the deflection angle α by analyzing the angle of the main axis with the sidewall, Θ , as the sperm or the cone travel beyond the corner (figure 7). The distance of the centroid (averaged over one beat) of the sperm to the corner defines the position s during the deflection event. When the sperm swims along the sidewall ($s < 0$), the orientation Θ fluctuates around the beat-pattern opening angle (see appendix A). Starting with the head passing the tip of the corner, the main axis rotates, until subsequently it plateaus after the sperm has passed the corner. This retroactively justifies the definition of the deflection angle α in section 3.1. Sperm with perpendicular beat-plane orientation turn faster over a shorter length scale, while sperm with parallel beat-plane orientation turn slower over a longer length scale. Here, the average deflection of sperm with perpendicular beat-plane orientation is two times larger than for sperm with parallel beat-plane orientation.

The cone model describes the change of orientation for both beat-plane orientations quite well (figure 7). In the perpendicular case, an effective opening angle $\delta_{\perp} = 14^\circ$ and cone length of $L'_{\perp} = 15 r_h$ matches the deflection of the full hydrodynamic model. Here, the self-propelled cone model nicely corresponds to the beat-shape envelope of the sperm (figure 8). For a sperm with parallel oriented beat plane, we expect much less influence of the steric interaction and more dominance of the hydrodynamic interaction. The simple steric model with opening angle $\delta_{\parallel} = 6^\circ$ and length $L'_{\parallel} = 15 r_h$ again captures the averaged motion quite well. The gap between the average orientation of the sperm and the self-propelled cone indicates a small additional



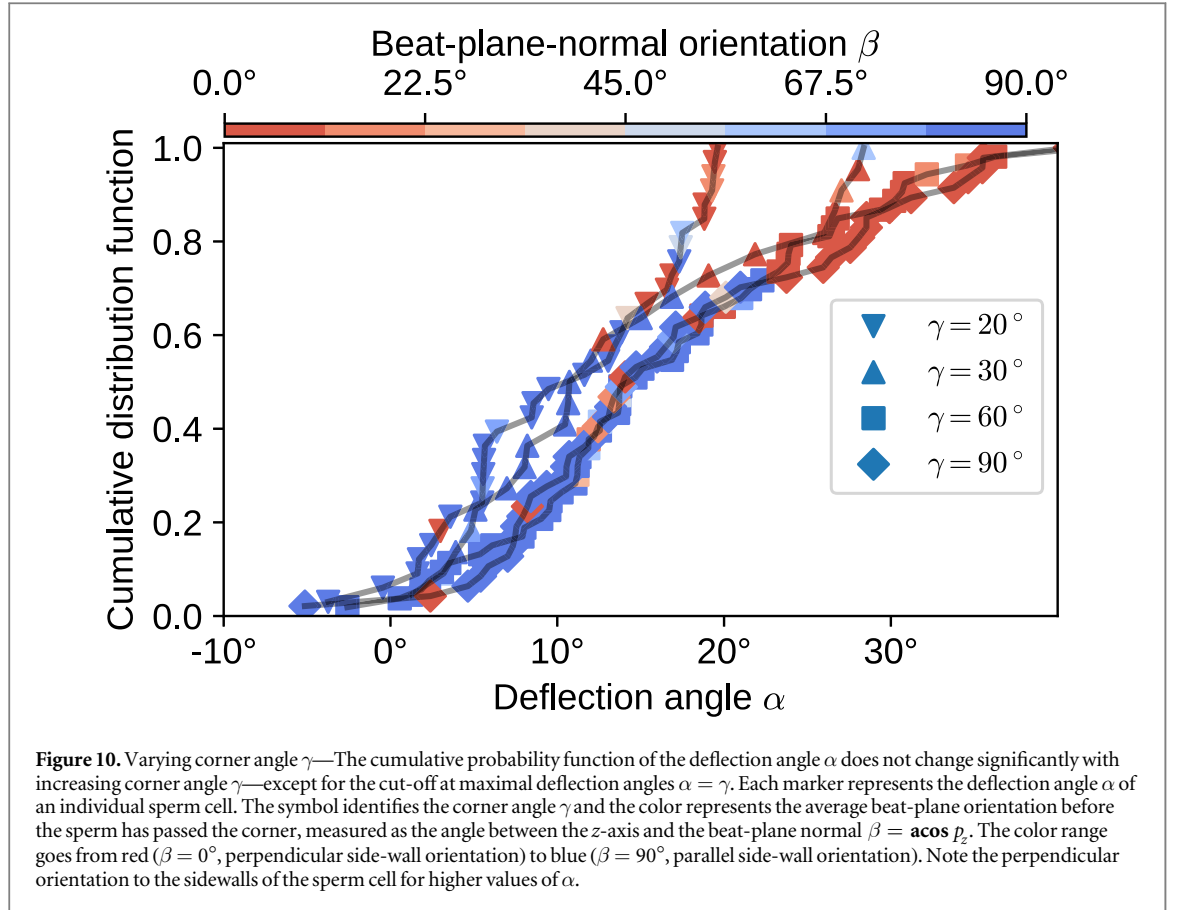
hydrodynamics contribution. As already suggested in [16], the effective opening angles indicates a hydrodynamic repulsion of the sperms tail.

The beating is reflected in the distribution of the inclination angles Θ (figure 3). Indeed, sperm with parallel and perpendicular beat-plane orientation have a large difference in inclination angle (figure 9). For perpendicular beat-plane orientation, the inclination angle is almost equally distributed between $\Theta_{\perp} = 3^{\circ}$ to 23° , which can be understood by the beating of the sperm that constantly changes the orientation of the main axis and thereby interacts sterically with the sidewall. The regular beating of the flagellum creates a broad, almost uniform distribution. In contrast, the inclination of sperm with parallel beat-plane orientation is almost Gaussian distributed around an average inclination of $\langle \Theta_{\parallel} \rangle = 3 \pm 5^{\circ}$. In the latter case, the inclination seems to be mainly caused by hydrodynamic interactions and thermal noise.

3.3. Shallow corner angles and rounded corners

To go a step further, we consider more complex sidewall patterns that are interesting for the design of microchannels for various applications: shallow angles and rounded corners (see section 2.4). The success of the simple self-propelled cone model in predicting sperm deflection at sharp corners, suggests to apply and verify this approach to these new channel designs.

For one, we vary the corner angle: the cone model would not notice the more shallow angle, until it collides with the subsequent wall. In contrast, long-range hydrodynamic interactions might be expected to help the cell to ‘feel’ the presence of the distant sidewall, and thus scatter differently. The cone model indeed predicts that shallow corner angles only impose an upper limit on the deflection distribution, because deflection angles larger than the corner angle are not possible. In the latter case, the sperm remains at the originating sidewall, i.e. it does not cross the channel after deflection. The cumulant of the deflection-angle probability distributions (figure 10), nicely demonstrates this behavior: the cumulants are nearly identical for deflection angles smaller than the corner angles, and increase steeply thereafter. Thus, the beat-plane orientation still dominates the deflection-angle probability distributions (figure 10), and hydrodynamic interactions seem to play only a minor role. For $\alpha = \gamma$ the sperm cell turns entirely around the corner and stays at the originating sidewall. However, α can be slightly larger than γ , due to the finite distance between the sperm cell and the wall.



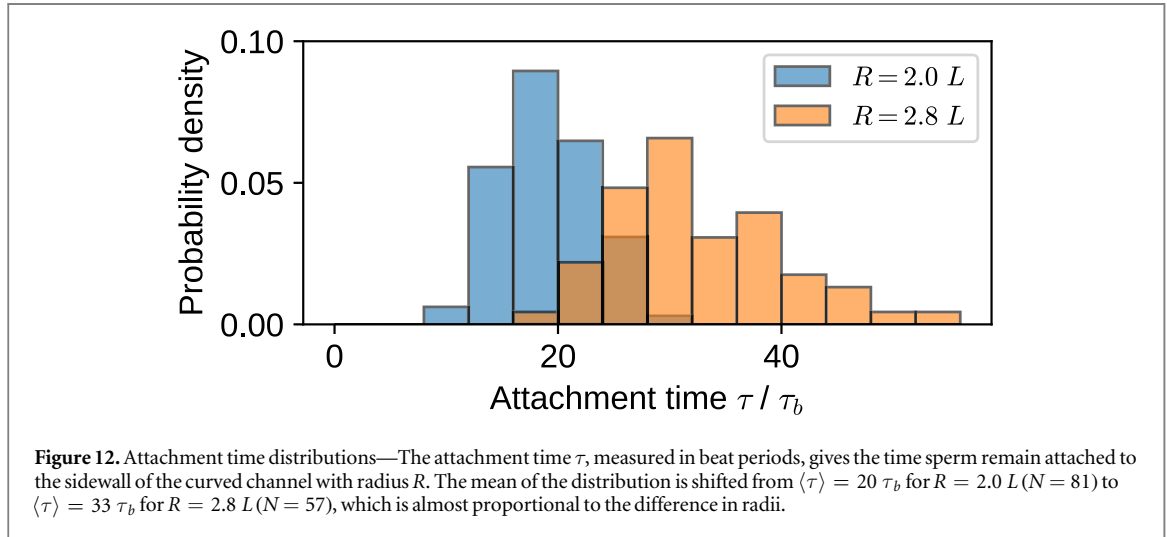
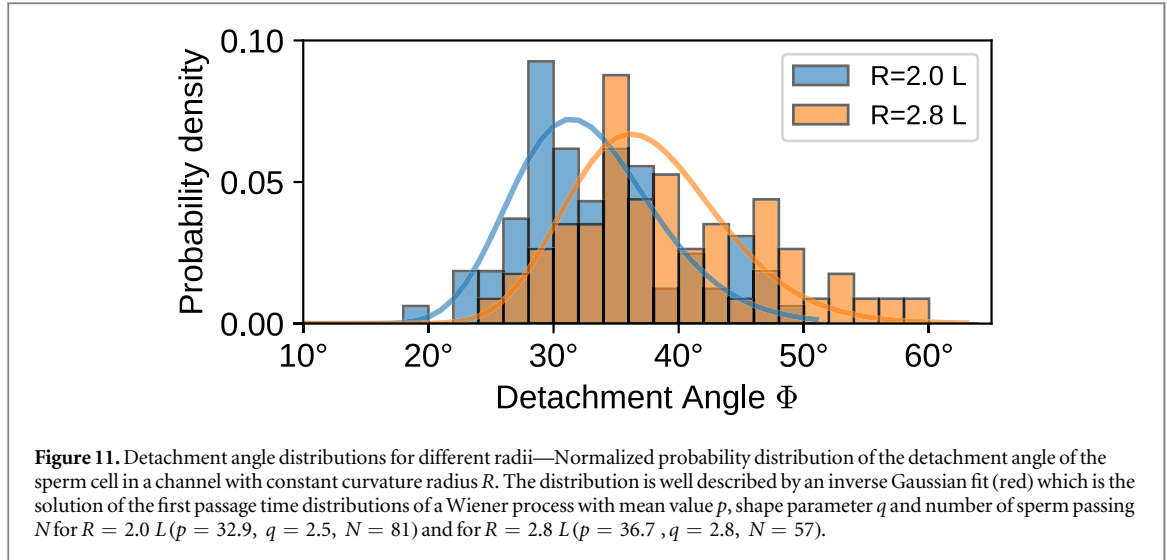
A second interesting prediction arises from the cone model: if confronted with a curved wall, a self-propelled cone attaches firmly to it, depending on the opening angle versus the radius of curvature [22]. The critical radius of curvature is expected to be $R_{||}^c = L'/(2\delta_{||}) = 4.2 L$ for the parallel orientation and a radius of curvature above $R_{\perp}^c = L'/(2\delta_{\perp}) = 1.2 L$ for the perpendicular orientation. We thus explore a novel channel design, where sperm swim along sidewalls with regions of alternating, constant curvature, as introduced in section 2.4. By tuning the radius of curvature R of the curved segments, we expect to control the probability of a sperm cell to stay attached. We choose $R = 2 L$ and $R = 2.8 L$ (larger radii of curvature are unfortunately computationally unfeasible). We thus expect perpendicular aligned sperm to remain attached, and parallel aligned sperm to detach from the originating wall. Interestingly, the observed behavior is more complex.

Because the detachment at curved corners can happen along the entire surface, no unique detachment point can easily be defined anymore. Instead, the attachment strength is quantified by measuring the length of the path along the quarter-circle before detachment. The region of constant, non-zero curvature starts at $\Phi = 0^\circ$. After the sperm cell swims into the region of constant curvature, it continues to swim along the curved sidewall until it orients away from the surface and eventually detaches. The sperm is considered as detached when the centroid of the sperm cell is more than $8 r_h$ away from the curved surface. This point then defines the detachment angle Φ .

Figure 11 shows the probability distributions of these detachment angles for a radius of curvature of $R = 2 L$ and $R = 2.8 L$, where the mean detachment angle $\langle \Phi \rangle$ increases slightly from about $\langle \Phi \rangle = 33^\circ$ to $\langle \Phi \rangle = 38^\circ$ respectively. However, no sperm cell swims around the curved region entirely, even though the steric argument predicts complete attachment for the perpendicular orientation in both cases. The reason for this is the destabilization of the perpendicular beat-plane orientation by the curvature of the sidewall. The dominant mode of detachment is that perpendicular oriented sperm rotates into the parallel orientation, and then detaches from the sidewall. The same detachment angle corresponds to longer attachment times for larger R (figure 12). Indeed, the mean attachment time τ increases by a factor of 1.67 from $R = 2 L$ to $R = 2.8 L$.

Spagnolie *et al* [23] studied the very similar problem of a hydrodynamic dipole swimmer trapped at the surface of a cylinder, and analyzed it as a Wiener process with drift which predicts an inverse Gaussian, $f(\Phi) = q/(2\pi\Phi^3) \exp\{-q(\Phi - n)^2/(2p^2\Phi)\}$, as the solution of the first passage time. Indeed, our detachment-angle distribution is also well described by an inverse Gaussian for both radii of curvature (figure 11).

Although the inverse Gaussian describes the detachment angle distribution very well, the detachment process differs in our case. As explained above, the detachment is dominated by the reorientation of the beat



plane. This detachment process is hindered in shallower channels. Indeed, we see a rapid change in crossing probability at a critical channel height h , which depends on the imposed wavelength λ (figure 13). The wavelength dependence of the crossing probability will be discussed further in context of the effects of the beat pattern, see section 3.4.

3.4. Effects of the beat pattern

The dominant role of steric effects, determined by the beat envelope, suggests a strong influence of the beating pattern on wall adherence and wall scattering. Thus we consider the beat pattern in more detail. First, the beat pattern of freely swimming sperm is simulated for varying wavelength λ in a large simulation box of size $L_x = 35 r_h$, $L_y = 35 r_h$ and $L_z = 35 r_h$ with periodic boundaries in x , y and z -directions. Their beat pattern is quantified by the beat-shape envelope which has two opening angles: the in-plane opening angle $\delta_b(t)$ and the out-of-plane opening angle $\delta_p(t)$ (see appendix A for details). Second, we test the dominant effect of the beat plane on swimming along the curved channels.

Figure 14 shows the increase of the opening angle δ_b with increasing wavelength λ . When the wavelength increases above a threshold of $\lambda = 0.79 L$, the flagellum buckles under the load of the pushing and viscous forces (as suggested in [24]) and exhibits an out-of-plane component, leading to a three-dimensional beat pattern (top of figure 14, supplementary movie 2). In the planar beating regime, the out-of-plane opening angle, δ_p , is negative, since the head radius is much larger than the radius of the straight flagellum (see appendix A). Here, for $\delta_p < 0$, the in-plane opening angle δ_b increases linearly with the wavelength, $\delta_b(\lambda) = 30^\circ \lambda/L - 6^\circ$. In the three-dimensional beat regime, the out-of-plane opening angle δ_p increases, while the in-plane opening angle stays constant. Although this needs further investigation, we will focus here on the effect of the beat-shape envelope on the wall attraction in close confinements.

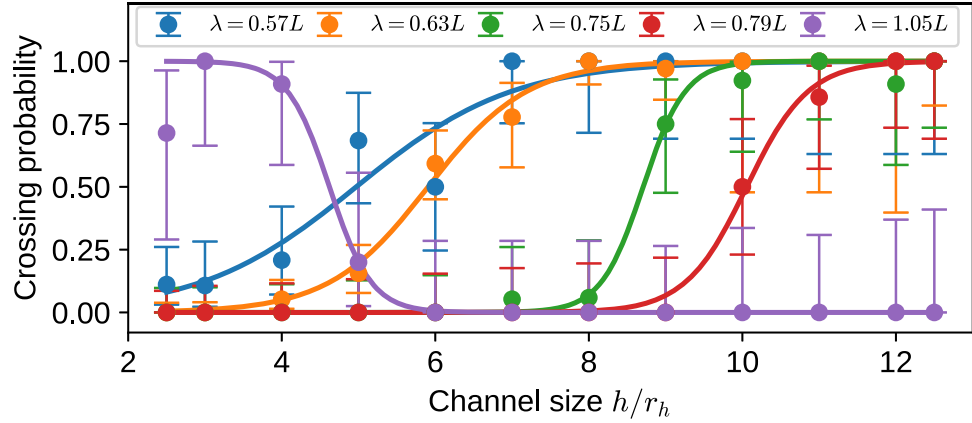


Figure 13. Channel-crossing probability—The crossing probability of a sperm with imposed beating wavelength λ at the rounded corners for different channel heights h . Error bars are 95% confidence intervals. The solid line shows a sigmoidal fit. For planar beating sperm, with $\lambda \leq 0.8 L$, the crossing probability increases rapidly when the channel height h allows the turning of the beat plane. For three-dimensional beat patterns, with $\lambda = 1.05 L$, the confinement has the opposite effect; the crossing probability drastically decreases with channel height.

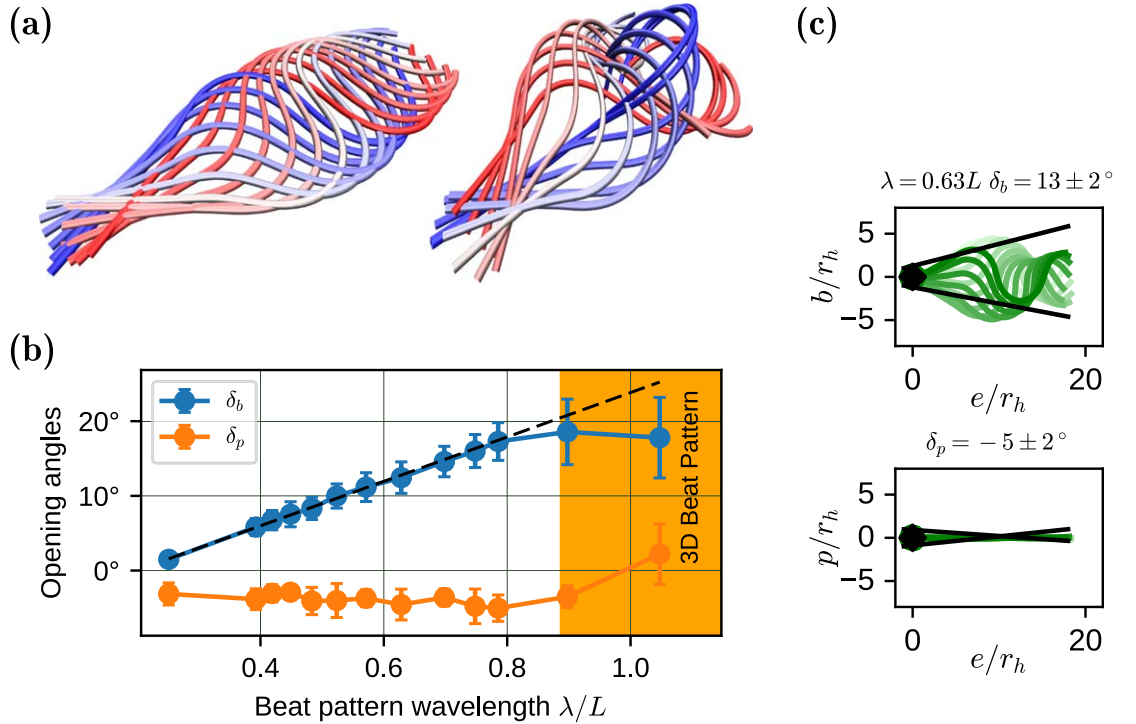
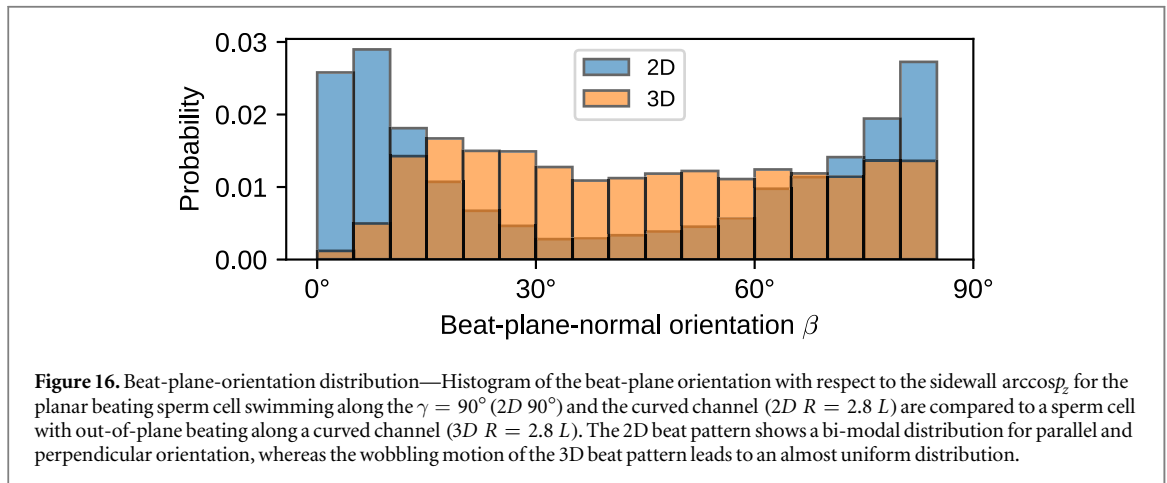
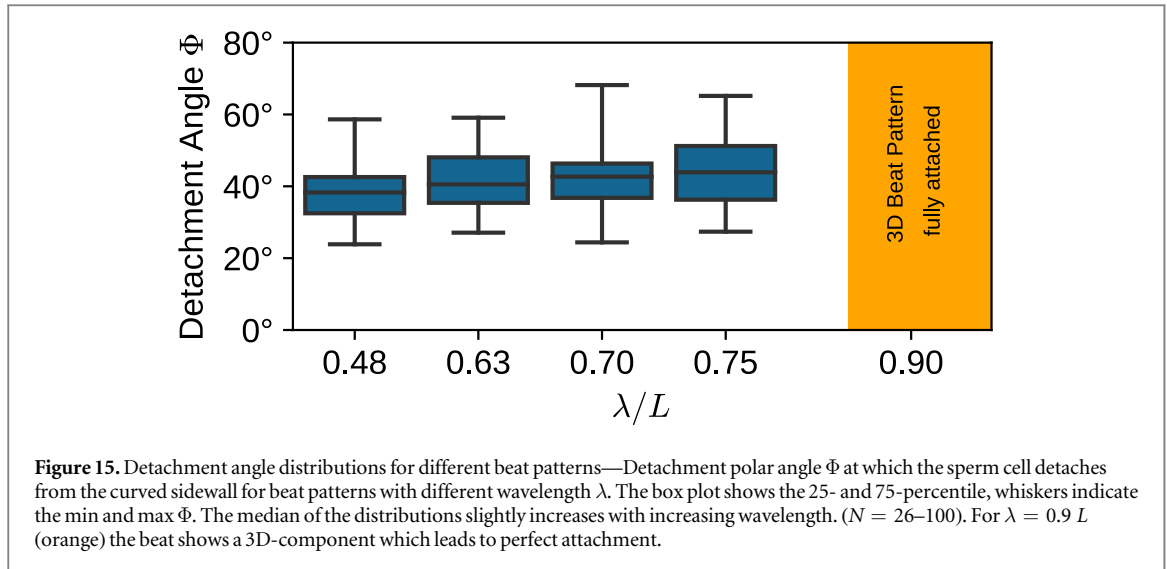


Figure 14. Beat shape—(a) Snapshots show a planar ($\lambda = 0.63 L$) and a three-dimensional ($\lambda = 1.05 L$) beat pattern in the lab frame. The snapshots are colored by time from red over gray to blue. Sperm head (not shown) is on the bottom-left end of the flagellum. A movie of the three-dimensional beat is shown supplementary movie 2. (b) The in-plane opening angle δ_b of the beat-shape envelope increases linearly with wavelength λ until the out-of-plane opening angle δ_p starts to increase ($\lambda \geq 0.79 L$). Error bars indicate the standard deviation when averaged over several beats. The increase of the in-plane opening angle is $\delta_b/\lambda = 30^\circ/L$. (c) Visualization of the beat pattern for the planar beating sperm cell with $\lambda = 0.63 L$ explaining the in-plane opening angle δ_b and out-of-plane opening angle δ_p (see also appendix A).

We want to mention parenthetically that the shape of the planar beat in figure 14 (top) agrees well with the beat shapes of human sperm tethered to a wall at its head, as observed experimentally and in resistive-force simulations [17].

In deep channels, even though the increasing wavelength increases the opening angle δ_b of the beat pattern (figure 14), only a minor influence on the detachment point distribution at rounded corners is observed for $\lambda \leq 0.7 L$ (figure 15). Conversely, the behavior changes abruptly to perfect attachment for wavelengths $\lambda \geq 0.9 L$. This sudden transition coincides with the instability of the planar beat pattern. In



contrast, in shallow channels (figure 13), the attachment–detachment behavior is inverted. For planar beating ($\lambda \leq 0.8 L$), sperm stay perfectly attached to the sidewall below a critical channel height h_c , whereas in the three-dimensional beat regime ($\lambda \geq 0.9 L$), they stay attached above a critical channel height h_c . In the planar-beat regime, the restriction of the beat-plane orientation perpendicular to the sidewall enforces a strong steric repulsion of the flagellum and the sidewall. A larger wavelength λ increases the beat-shape opening angle δ_b (figure 14), which increases the critical channel height h_c that allows the beat plane to rotate into a parallel orientation.

Together with the results for shallow channels, this provides a consistent picture of how sperm travel around rounded corners: the planar beating pattern in a curved channel starts with a similar bi-modal distribution of beat-plane orientations as for the sharp corners (figure 16). However, the curvature of the sidewall, destabilizes the perpendicular beat-plane orientation with the sidewall. When the sperm rotates to a parallel-aligned beat plane, the sperm starts to detach from the sidewall (supplementary movie 3). For three-dimensional beating sperm cells, the beat-plane orientation keeps wobbling between $25^\circ < \arccos p_z < 90^\circ$ (figure 16). This exposes the asymmetry of the beating to the sidewall and therefore rotates the main elongation axis back toward the surface (supplementary movie 4). The shallow channels archive the same results by enforcing the exposure of the asymmetry of the beating to the sidewall due to the confinement.

This picture also explains the almost unchanged detachment-angle distribution for increasing wavelength for $\lambda < 0.9 L$. Even though the increasing asymmetry of the beat pattern increases the surface attachment of the perpendicular orientated sperm cell, the detachment is dominated by the rotation of the destabilized perpendicular orientation.

4. Summary and discussion

We have studied the deflection of sperm off sharp and rounded corners in zigzag channels. Our hydrodynamic simulations reproduce the broad deflection-angle distribution found in experiments of human sperm cells. Our results underline the importance of a combination of hydrodynamic and steric interactions. We show that the beat-shape orientation is of critical importance for surface attraction and subsequent scattering off corners. Due to the cone-like structure of the beat-shape envelope, the head is closer to the wall than the tail of the sperm. This inclines the principle axis of the sperm cell toward the wall, which leads to a force component that pushes the sperm cell toward the sidewall. Once the sperm cell passes the tip of the corner, it is free to move in the sidewall direction and therefore partially turns around the corner. When the beat plane is perpendicular oriented to the channel wall, the deflection is dominated by steric interaction. We find that the average deflection of the sperm cell is reproduced by a self-propelled cone, where the opening angle of the cone matches the beat-shape-envelope inclination of the sperm cell with respect to the sidewall.

When the beat-plane is parallel oriented to the channel wall, the flagellum hardly touches the wall. Interestingly, the main axis of the sperm cell is still slightly inclined [16], which allows the construction of an effective steric model that is able to approximately describe the deflection. However, the active beating of the sperms tail and the thermal noise of the simulation leads to large fluctuations of the individual deflections.

At curved corners, sperm cells detach by rotating to the parallel orientation, thus exposing the less asymmetric side of the beat pattern. This rotation can be inhibited by very shallow channels, leading to perfect adhesion to the curved sidewall. Alternatively, above a critical wavelength of $\lambda = 0.79 L$, a buckling instability occurs which renders the beat pattern three-dimensional and leads to a wobbling of the entire sperm cell around the main axis. This dramatically increases surface attraction.

Our simulation results pose some interesting questions about how surface interactions guide microswimmers, in particular sperm cells, through complex and highly confined geometries. As shown, the wavelength-dependent instability toward a three-dimensional beat pattern strongly enhances surface attraction, which may explain why sperm can easily follow the windings of the Fallopian tube. Therefore, the beat shape influences the fitness of sperm beyond simple propulsive effects.

Our results emphasize the importance of resolving a three-dimensional shape of the beat pattern and study sperm swimming in shallow channels. Such a setup could be exploited to filter sperm cells by translating properties of the beat pattern to angular deflection. Considering the strong attraction of three-dimensional beating sperm cells, the recently proposed design of teardrop-shaped posts seems to be particularly promising [25]. The teardrops have a large radius of curvature at the bottom and a small radius of curvature at the top, and thereby allow for alignment of swimmers along the low curvature regions and detachment when approaching the high curvature regions. When tuned accordingly, only sperm with large wavelength that show a three-dimensional beat pattern align along the direction of the teardrop, whereas sperm cells with smaller wavelength, and thus planar beat, are not.

A detailed experimental investigation of the beat pattern of human sperm close to surfaces reveals a switch between three-dimensional spiraling and two-dimensional slithering motion [26–28]. This switching between an extended three-dimensional beat and a two-dimensional beat influences sperm motility in confinement and is an interesting topic to study experimentally.

Acknowledgments

Financial support by the Deutsche Forschungsgemeinschaft via the DFG priority program SPP 1726 ‘Microswimmers’ is gratefully acknowledged. The authors gratefully acknowledge the computing time granted through JARA-HPC on the supercomputer JURECA [29] at Forschungszentrum Jülich. We thank L Alvarez, A Gong and U B Kaupp (Forschungszentrum caesar, Bonn) for helpful discussion. Relevant simulation data is available in an external repository at [10.5281/zenodo.2222434](https://doi.org/10.5281/zenodo.2222434) [30].

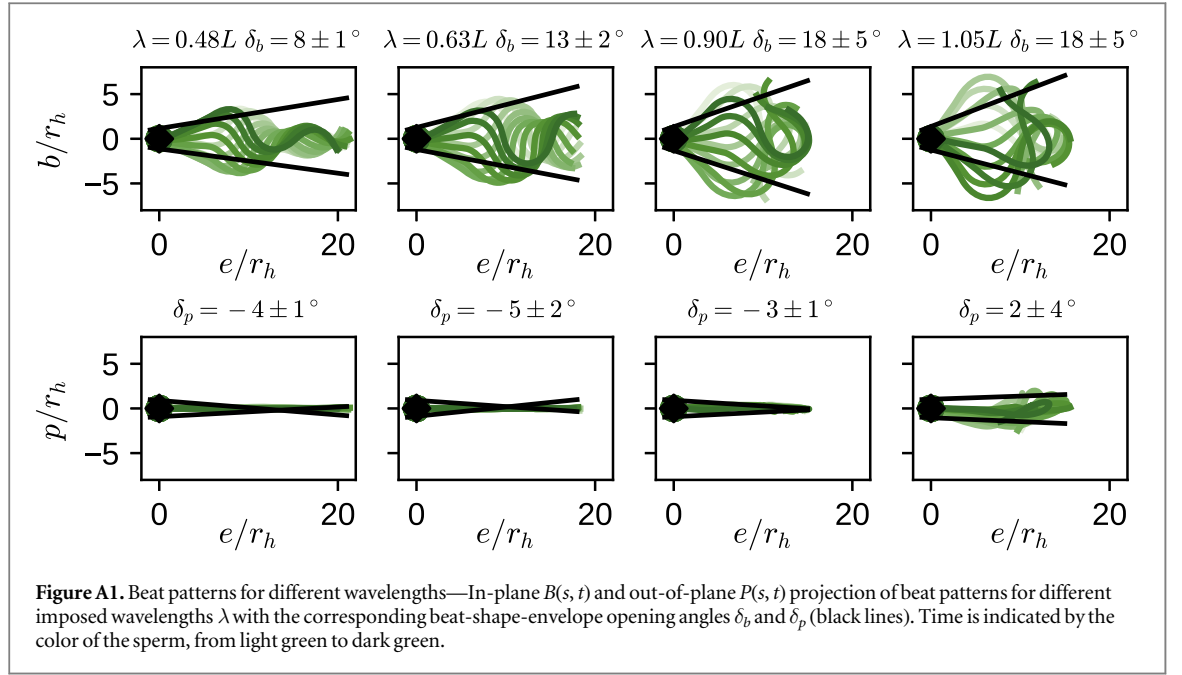
Appendix A. Quantification of the beat-shape envelope

The flagellum is quantified by the space curve $\mathbf{r}(s, t)$. Translation motion is subtracted so that $\mathbf{r}(0, t) = 0$. The in-plane elongation $B(s, t)$ and the out-of plane $P(s, t)$ follow by the corresponding b - and p -projection:

$$B(s, t) = \mathbf{r}(s, t) \cdot \mathbf{b}(t) \quad (\text{A.1})$$

$$P(s, t) = \mathbf{r}(s, t) \cdot \mathbf{p}(t). \quad (\text{A.2})$$

The beat shape is quantified by the inclination angles of the line that encloses the beat pattern in the corresponding projection (figure A1). The line is constructed from the minimal (maximal) elongation of the



flagellum and the radius of the head r_h :

$$\tan \delta_b^+(t) = \frac{\max_{s'} B(s', t) - r_h}{E(s', t)} \quad (\text{A.3})$$

$$\tan \delta_b^-(t) = \frac{\min_{s'} B(s', t) + r_h}{E(s', t)}, \quad (\text{A.4})$$

where s' are the arc-length positions where $B(s)$ is maximal δ_b^+ or minimal δ_b^- . Because both bounds have the same value with opposite sign, due to the axis symmetry of the beat pattern, the opening angle can be defined by taking the mean of their absolute values. The time dependence is omitted by averaging over several beats.

Appendix B. Cone model

In the cone model, we capture the two main effects leading to the deflection of the sperm cell at a corner. Its asymmetry with respect to the surface and the propulsion in the direction of its center line. Here, we followed closely the over-damped dynamics simulation without hydrodynamics and noise by Wysocki *et al* [22]. We model the cone as a series of N overlapping spheres. Their radius increases linearly from the radius r_0 of the first sphere to the radius r_1 of the last sphere. The spheres are held together by springs with a constant bond length $l_b = 0.25 r_h$ and a bending potential (the same as in the full sperm model). The distance between the center of the first sphere and the last one defines the length of the cone as $L' = l_b N$. Finally, this determines the cone opening angle $\tan \delta = (r_1 - r_0)/L'$.

Since simulations are performed in the limit of low Reynolds numbers, inertia effects can be ignored, and we have to solve the equation of over-damped motion,

$$\dot{\mathbf{r}}_i = \mu_0 (\mathbf{F}_d + \mathbf{F}_{\text{springs}} + \mathbf{F}_{\text{bending}}). \quad (\text{B.1})$$

The cone-like swimmer is self-propelled in the direction of the connection vector between the center of the spheres \mathbf{e} . Therefore, we set $\mathbf{F}_d = f_0 \mathbf{e}$.

The mobility μ_0 of each sphere is kept constant. Only for bounce-back from interactions with the boundary of the channel the different radii are important. The interaction with the wall is modeled by checking the positions of the spheres in each time step. When they penetrate the wall, they are moved outwards along the normal of the corresponding wall. Since the normal is not well defined at the tip of the corner, here the radial vector between the center of the sphere and the tip is used.

Appendix C. Parameter list

Table C1 collects all parameters of our simulation approach, both for the sperm model as well as for the MPC fluid. All simulation parameters are given in MPC units, defined by $k_b T = 1$, $a = 1$ and $m = 1$.

Table C1. Simulation parameters for the sperm model and the MPC fluid.

Description	Symbol	Value
Beat frequency	ω	0.05
Beat wavelength	λ	0.1 (if not varied)
Beat amplitude	A	0.1
Spring constant	γ	20 000
Spring constant (head)	γ_c	2000
MD particle mass	—	5
Free path length	λ_c	0.05
Fluid particle density	—	10


Table C2. Equations defining the sidewall of the zigzag channels.

Corner angle γ	$y(x)$	y_0 lower	y_0 upper
5°	$36(\arcsin(\cos(2\pi x/\text{size}x + \pi))/2\pi + 0.25)$	1	101
10°	$71(\arcsin(\cos(2\pi x/\text{size}x + \pi))/2\pi + 0.25)$	1	103
15°	$108(\arcsin(\cos(2\pi x/\text{size}x + \pi))/2\pi + 0.25)$	1	106
30°	$230(\arcsin(\cos(2\pi x/\text{size}x + \pi))/2\pi + 0.25)$	1	117
45°	$400(\arcsin(\cos(2\pi x/\text{size}x + \pi))/2\pi + 0.25)$	0	150

The sidewalls of the rectangular channel are defined by the following functions $y(x) + y_0$ (see table C2), where y_0 corresponds to the offset of the sidewall. For the lower one, we choose $y_0 = 1$ and the upper one is placed at $y_0 = 106$. Note that for $\gamma = 45^\circ$ the upper (lower) sidewall is limited to a maximum (minimum) value of $y = 330$ ($y = 21$), in order to flatten the pointed angle of the outward corner.

ORCID iDs

Jens Elgeti  <https://orcid.org/0000-0001-7300-0923>

Gerhard Gompper  <https://orcid.org/0000-0002-8904-0986>

References

- [1] Elgeti J and Gompper G 2016 Microswimmers near surfaces *Eur. Phys. J. Spec. Top.* **225** 2333–52
- [2] Gaffney E A, Gad  lha H, Smith D, Blake J R and Kirkman-Brown J 2011 Mammalian sperm motility: observation and theory *Annu. Rev. Fluid Mech.* **43** 501–28
- [3] Kaupp U B, Kashikar N D and Weyand I 2008 Mechanisms of sperm chemotaxis *Annu. Rev. Physiol.* **70** 93–117
- [4] Alvarez L, Friedrich B M, Gompper G and Kaupp U B 2014 The computational sperm cell *Trends Cell Biol.* **24** 198–207
- [5] Miki K and Clapham D E 2013 Rheotaxis guides mammalian sperm *Curr. Biol.* **23** 443–52
- [6] Kantsler V, Dunkel J, Blayney M and Goldstein R E 2014 Rheotaxis facilitates upstream navigation of mammalian sperm cells *eLife* **3** e02403
- [7] Zhang Z, Liu J, Meriano J, Ru C, Xie S, Luo J and Sun Y 2016 Human sperm rheotaxis: a passive physical process *Sci. Rep.* **6** 23553
- [8] Rothschild L 1963 Non-random distribution of bull spermatozoa in a drop of sperm suspension *Nature* **200** 381–381
- [9] Elgeti J, Winkler R G and Gompper G 2015 Physics of microswimmers—single particle motion and collective behavior: a review *Rep. Prog. Phys.* **78** 056601
- [10] Guidobaldi A, Jeyaram Y, Berdakin I, Moshchalkov V V, Condat C A, Marconi V I, Giojalas L and Silhanek A V 2014 Geometrical guidance and trapping transition of human sperm cells *Phys. Rev. E* **89** 032720
- [11] Nosrati R, Vollmer M, Eamer L, San Gabriel M C, Zeidan K, Zini A and Sinton D 2014 Rapid selection of sperm with high DNA integrity *Lab Chip* **14** 1142–50
- [12] Eamer L, Vollmer M, Nosrati R, San Gabriel M C, Zeidan K, Zini A and Sinton D 2016 Turning the corner in fertility: high DNA integrity of boundary-following sperm *Lab Chip* **16** 2418–22
- [13] Nosrati R, Graham P J, Liu Q and Sinton D 2016 Predominance of sperm motion in corners *Sci. Rep.* **6** 26669
- [14] Denissenko P, Kantsler V, Smith D J and Kirkman-Brown J 2012 Human spermatozoa migration in microchannels reveals boundary-following navigation *Proc. Natl Acad. Sci. USA* **109** 8007–10
- [15] Kantsler V, Dunkel J, Polin M and Goldstein R E 2013 Ciliary contact interactions dominate surface scattering of swimming eukaryotes *Proc. Natl Acad. Sci. USA* **110** 1187–92
- [16] Elgeti J, Kaupp U B and Gompper G 2010 Hydrodynamics of sperm cells near surfaces *Biophys. J.* **99** 1018–26
- [17] Saggiorato G, Alvarez L, Jikeli J F, Kaupp U B, Gompper G and Elgeti J 2017 Human sperm steer with second harmonics of the flagellar beat *Nat. Commun.* **8** 1415
- [18] Lighthill J 1975 *Mathematical Biofluidynamics* (Philadelphia, PA: SIAM)
- [19] Ripoll M, Mussawisade K, Winkler R G and Gompper G 2005 Dynamic regimes of fluids simulated by multiparticle-collision dynamics *Phys. Rev. E* **72** 016701

- [20] Gompper G, Ihle T, Kroll D M and Winkler R G 2009 Multi-particle collision dynamics: a particle-based mesoscale simulation approach to the hydrodynamics of complex fluids *Adv. Polym. Sci.* **221** 1–87
- [21] Lamura A, Gompper G, Ihle T and Kroll D M 2001 Multi-particle collision dynamics: flow around a circular and a square cylinder *Europhys. Lett.* **56** 319–25
- [22] Wysocki A, Elgeti J and Gompper G 2015 Giant adsorption of microswimmers: duality of shape asymmetry and wall curvature *Phys. Rev. E* **91** 050302
- [23] Spagnolie S E, Moreno-Flores G R, Bartolo D and Lauga E 2015 Geometric capture and escape of a microswimmer colliding with an obstacle *Soft Matter* **11** 3396–411
- [24] Gadelha H, Gaffney E A, Smith D J and Kirkman-Brown J C 2010 Nonlinear instability in flagellar dynamics: a novel modulation mechanism in sperm migration? *J. R. Soc. Interface* **7** 1689–97
- [25] Davies Wykes M S, Zhong X, Tong J, Adachi T, Liu Y, Ristroph L, Ward M D, Shelley M J and Zhang J 2017 Guiding microscale swimmers using teardrop-shaped posts *Soft Matter* **13** 4681–8
- [26] Nosrati R, Driouchi A, Yip C M and Sinton D 2015 Two-dimensional slither swimming of sperm within a micrometre of a surface *Nat. Commun.* **6** 8703
- [27] Su T W, Xue L and Ozcan A 2012 High-throughput lensfree 3D tracking of human sperms reveals rare statistics of helical trajectories *Proc. Natl Acad. Sci. USA* **109** 16018–22
- [28] Cosson J, Huitorel P and Gagnon C 2003 How spermatozoa come to be confined to surfaces *Cell Motil. Cytoskeleton* **54** 56–63
- [29] Jülich Supercomputing Centre 2018 JURECA: modular supercomputer at Jülich Supercomputing Centre *J. Large-Scale Res. Facil.* **4** A132
- [30] Rode S, Elgeti J and Gompper G 2018 Sperm motility in modulated microchannels *Data Set (Zenodo)* [doi:10.5281/zenodo.2222434]